PACIFIC EARTHQUAKE ENGINEERING
RESEARCH CENTER

Documentation of Strengths and Weaknesses of Current Computer Analysis Methods for Seismic Performance of Reinforced Concrete Members

William F. Cofer

PEER 1999/07
NOVEMBER 1999

Documentation of Strengths and Weaknesses of Current Computer Analysis Methods for Seismic Performance of Reinforced Concrete Members

William F. Cofer
Department of Civil and Environmental Engineering
Washington State University
Pullman, Washington

PEER Report 1999/07
Pacific Earthquake Engineering Research Center
College of Engineering
University of California, Berkeley
November 1999

ABSTRACT

One of the future needs of the engineering community is a general computational platform for the seismic analysis of structures, structural components, and the interaction between structures and surrounding soil. However, before a large effort is expended, a thorough evaluation of current capabilities is required to establish the state of the art and to determine the direction that should be taken with regard to design needs and analytical approaches. A specific area of interest is the analysis of reinforced concrete components, including cracking and crushing of concrete and yield of steel. The focus of the work of this report was to perform an evaluation of current capabilities in this area by applying several existing software packages to a benchmark problem. Data from a set of recent experimental tests involving the flexural and shear performance of a reinforced concrete column were obtained. Cyclic and monotonic load cases were performed for several types of analysis using a degrading plastic hinge model, a fiber beam model, and a detailed three-dimensional finite element model. Details of the data preparation and analysis results are presented. Reasonable results were obtained from all models to varying degrees, but the three-dimensional finite element model was unable to provide meaningful solutions in the inelastic range due to numerical difficulties. Therefore, either the use of the degrading hinge model or the fiber beam model is recommended for practical structural analysis.

ACKNOWLEDGMENTS

This work was supported in part by the Pacific Earthquake Engineering Research Center through the Earthquake Engineering Research Centers Program of the National Science Foundation under Award number EEC-9701568.

CONTENTS

LIST OF FIGURES

LIST OF TABLES

1 Introduction

Many seismic analyses involve the need to model concrete structural components. Nonlinear effects in reinforced concrete during seismic activity result from a number of mechanisms, including concrete crushing and cracking; yield and strain hardening of reinforcement; buckling of reinforcement; bond slip; interaction between axial force, biaxial bending, biaxial shear force, and torsional moment; and degradation of stiffness and strength under cyclic loads. Analyses of concrete structures may be performed at a number of levels. For the simplest approach, reinforced concrete beams and columns are modeled as traditional beam elements, with material nonlinearity lumped at discrete plastic hinges. Refinements would include a relationship between column axial force and inelastic bending moment, an algorithm for proper hysteretic behavior, and a damage coefficient to consider strength and stiffness degradation. At the next level, a fiber model may be used for structural members, in which the material behavior is integrated over the cross section and along the length of the element. At the highest level, the concrete is modeled in detail with two or three dimensional solid elements, while the reinforcement is included with bar elements.

In order to evaluate the ability of existing software and analysis techniques to accurately model the behavior of actual reinforced concrete members, a benchmark test specimen was chosen. The test sequence was then modeled using the software *WSU-NEABS*, which employs lumped hysteretic plastic hinges, *ABAQUS*, with a fiber beam model, and *ABAQUS*, using nonlinear three-dimensional finite element analysis.

2 Benchmark Test Specimen

A series of tests were recently performed (Jaradat et al. 1998) to investigate the flexural and shear performance of typical existing bridge columns. The test arrangement was designed to represent the entire column from foundation to cap beam. The column was fixed at the base by a strong oversized footing, bolted to the test floor, and fixed at the top by an oversized cap which was attached to a W 14 x 61 steel beam and a tubular steel strut (5-inch o.d. x 0.25-inch w. t.), as shown in Figure 1. The column was circular with a diameter of 10 inches, and had a length of 70 inches. It was longitudinally reinforced with eight No. 4 ASTM Grade 40 steel bars (52 ksi measured yield strength) evenly spaced around the perimeter. Transverse steel reinforcement consisted of 9-gage wire in the form of circular hoops spaced at 3.85 inches on center. The column base incorporated a lap splice with a length of 20 longitudinal bar diameters. The concrete had a measured compressive strength of $f_c' = 4200$ psi.

Cyclic lateral load was applied by a computer-controlled actuator operating with displacement control, based on a pattern of progressively increasing displacements. In addition, an axial load of 19.0 kips was applied to the column, corresponding to $0.05 f_c' A_g$. The actual axial load resisted by the column varied according to the applied lateral load direction, due to framing action. This variation in column axial load would also occur in actual multi-column bridge bents under lateral loading.

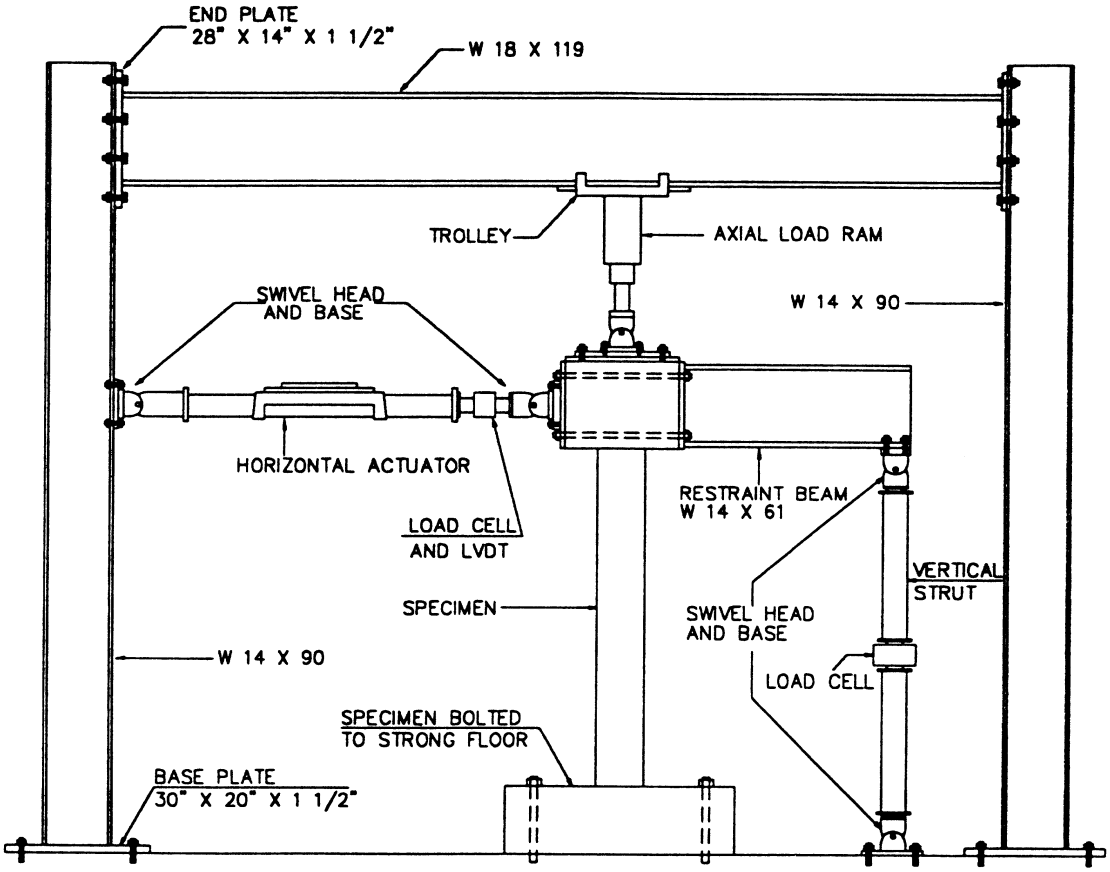

Figure 1. Test setup

2.1 Experimentally Observed Behavior

Specimen performance was evaluated on the basis of moment capacity, shear strength, displacement ductility, strength degradation, and hysteretic behavior. For this specimen, the measured yield displacement, Δ_y, was 0.56 inches. Vertical cracks in the bottom splice region and circumferential cracks in the top hinging section were observed while loading to a displacement level of $2\Delta_y$. The concrete cover started to spall off at $4\Delta_y$ in both the top and bottom hinge regions. Longitudinal bar buckling was observed in the top hinging region during cycling to $5\Delta_y$ and testing was stopped.

The hysteresis curves for the specimen are shown in Figure 2. The peak applied lateral load of 8.0 kips occurred at a displacement of 1.1 inches and was followed by a gradual degradation in load capacity. From the hysteresis curves for the top-section and bottom-section moments, it can be seen that the loss in capacity was primarily a result of degradation of the splice region at the base of the column. The top-section moment capacity showed a stable behavior until degradation started at a lateral displacement of 2.4 inches as a result of bar buckling.

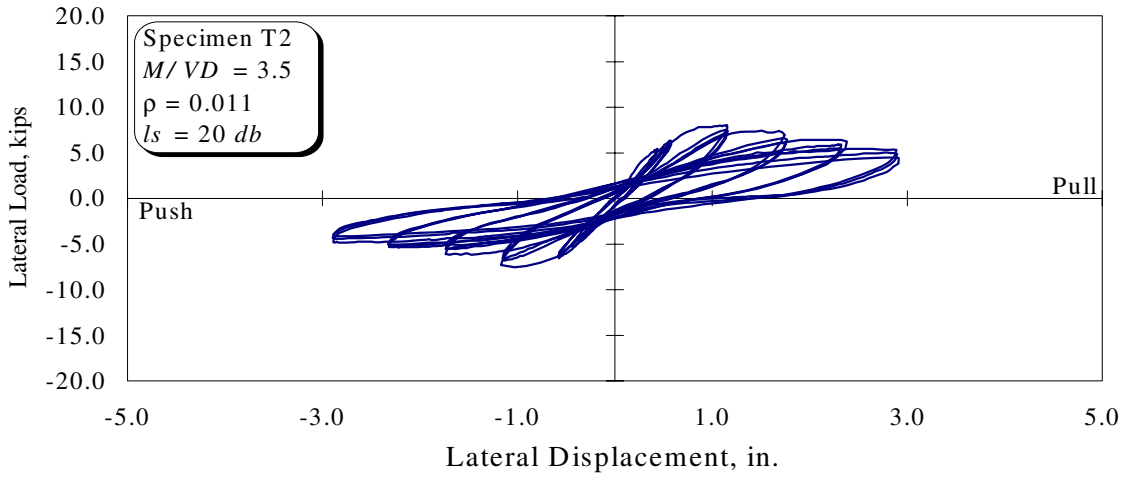

(a): Hysteresis curves of the lateral load vs. lateral displacement

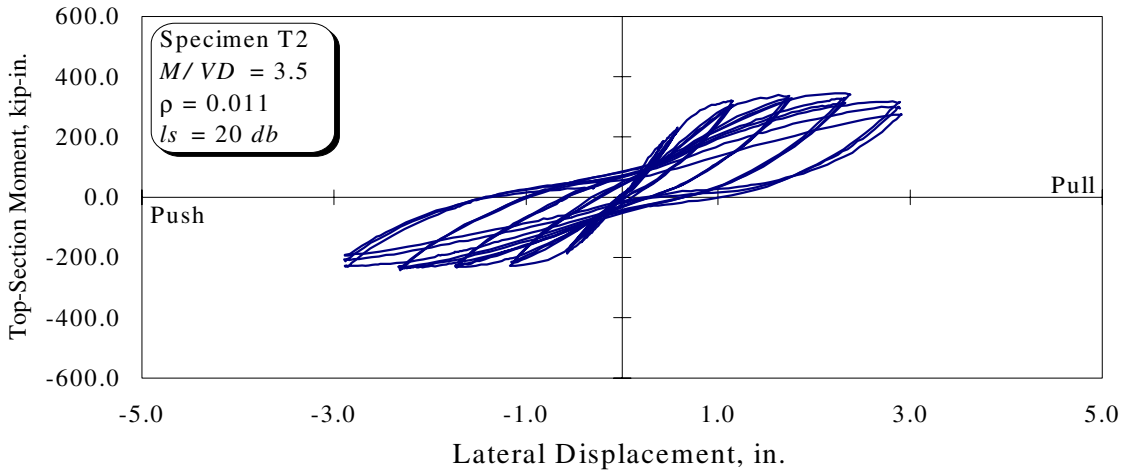

(b): Hysteresis curves of the top-section moment vs. lateral displacement

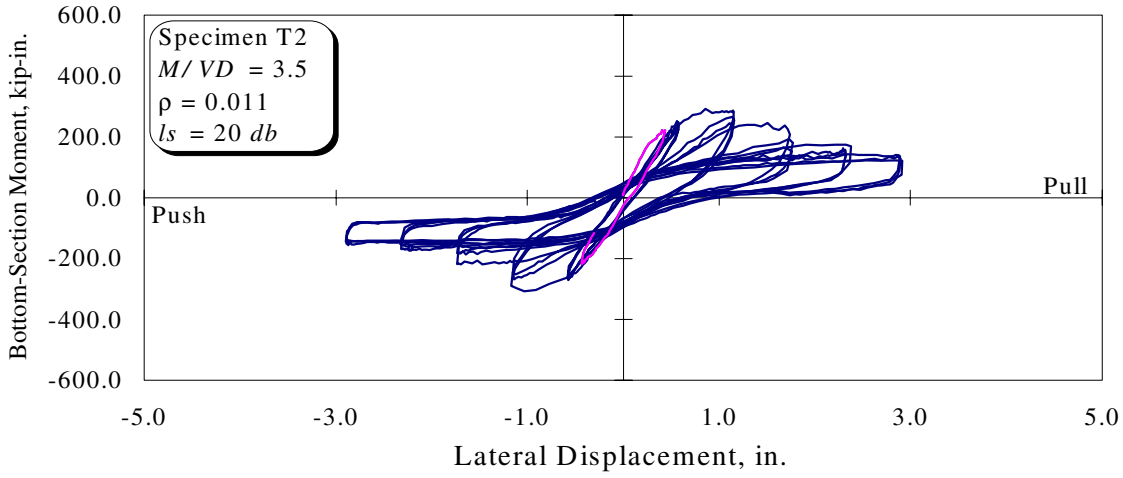

(c): Hysteresis curves of the bottom-section moment vs. lateral displacement

Figure 2. Hysteresis curves for the specimen (1 in. = 25.4 mm, 1 kip = 4.448 kN)

3 Software for Plastic Hinge Model

Tseng and Penzien developed a nonlinear mathematical model for bridge structural systems in 1973 in which an elasto-perfectly-plastic beam-column element and a bridge expansion joint element were presented (Tseng and Penzien 1973), called *NEABS* (*N*onlinear *E*arthquake *A*nalysis of *B*ridge *S*ystems). The program was later modified by Kawashima and Penzien (1976), and again by Imbsen, et al. (1978). To study energy absorption characteristics of highway bridges under seismic conditions, Imbsen and Penzien later presented a new nonlinear beam-column element that added kinematic hardening effects to *NEABS* (Imbsen and Penzien 1986). At the same time, a gapped tension-compression, tie-bar element was also developed for inclusion in the *NEABS* nonlinear expansion joint element. McGuire et al. (1994) modified the 1978 version of the program to include the effects of soil-structure interaction.

NEABS can evaluate a discrete bridge system subjected to applied dynamic loadings or prescribed support motions. The equations of motion in *NEABS* are solved by a step-by-step direct integration procedure. Either the constant acceleration or the linear acceleration method may be chosen for integration, and to increase the speed of convergence at each time step, an option is provided to subdivide the time step. However, this program has a major limitation in that the softening behavior of beam-columns due to damage is not considered. The structural elasto-plastic stiffness matrix for beam-column elements was derived for the original program by using plastic flow theory. It was assumed that the material behavior of the beam-column element was elastic-perfectly plastic (Fig. 3a), in which plastic hinges were point hinges (zero-length hinges). However, reinforced concrete members exhibit damage and softening behavior, i.e., decreasing bending moment at advanced flexural deformations before failure. Damage/softening is important for the dynamic analysis of pre-1971 designed highway bridges. Because most columns designed before 1971 had inadequate confinement and were lap-spliced at the connection zone between columns and footings (plastic hinge region), the flexural strength of columns in the potential plastic hinge region degrades rapidly with increased demand. The decrease of flexural strength of columns causes a redistribution of structural element forces, so that the seismic response of the entire highway bridge is significantly influenced. Moreover, an important aspect to dynamic column behavior is the degradation of stiffness when members are subjected to cyclic loadings, for which structural stiffness will decrease with reloading. The hysteresis rule used in the original version of *NEABS* is a conventional elastic-plastic model (Fig. 3b) that does not accurately represent the degradation of stiffness with increasing deformations for reinforced concrete. Therefore, the original *NEABS* program is not appropriate for evaluating the earthquake response for the highway bridges that were constructed before 1971.

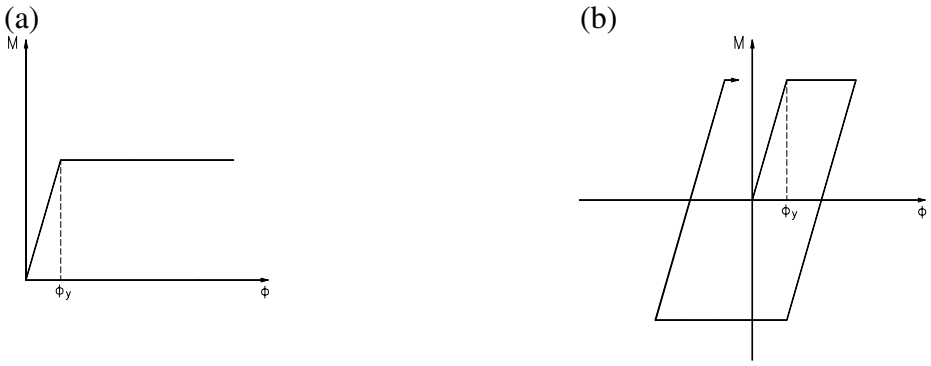

Figure 3. Moment-curvature relation and conventional hysteresis rule models used in original NEABS; (a) Moment-curvature relation; (b) Hysteresis rule

To overcome this limitation of *NEABS* and provide a realistic and practical method for the assessment of the effectiveness of different retrofit measures, a model for damage/softening behavior of beam-column elements based on an isotropic softening model with degradation of stiffness was proposed and then implemented into *NEABS*, as described in detail elsewhere (Cofer et al. 1997; Zhang et al. 1999). A basic description of the model is repeated below for completeness.

3.1 Beam-Column Element with Damage

For the elastic-perfectly plastic R/C beam-column element originally used in *NEABS*, the moment-curvature relation and hysteretic model in a one-dimensional force space are shown in Figure 3. However, most experimental results for R/C beams or columns subject to cyclic loading exhibit rather complicated behavior that includes such effects as rounding, pinching, and stiffness degradation (Imbsen and Penzien 1986). The most significant influence on structural analysis is stiffness degradation. According to experiments conducted by Priestley and Seible (1994), the elastic-perfectly-plastic model cannot represent the actual behavior if the plastic deformation is allowed to increase without limit. When plastic deformation at an end grows beyond a certain value (called critical curvature, ϕ_c), the material may undergo damage, which is represented by softening. In this stage, the moment decreases with an increase in plastic rotation.

Based on the experimental work done by Priestley, Seible, and Chai (1992), four models, as shown in Figure 4, were proposed to represent the strength and ductility of different plastic hinge conditions for column members. The parameter, μ_Δ, is the displacement ductility, defined as the ratio of maximum displacement at the top of a column divided by the yield displacement. The line (1) represents columns that have a comparatively well-confined section, in which the nominal moment capacity, M_n, will be reached at $\mu_\Delta = 1$, and then strain-hardening of flexural reinforcement and confinement effects will occur so that the moment reaches an overstrength moment capacity, M_0, that can be attained by moment-curvature analysis. This model is a typical representation of the relation between

strength and ductility for columns with sufficient confinement or retrofitting, i.e., steel jacketing, etc.

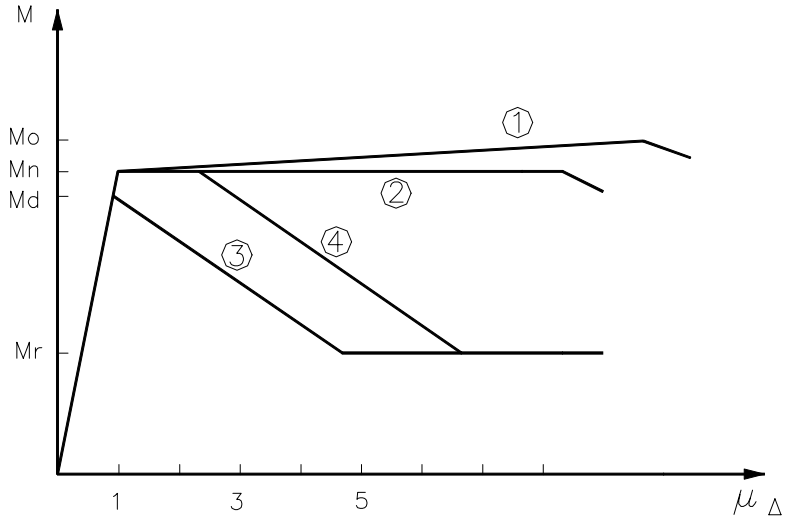

Figure 4. Flexural strength and ductility of sections (Priestley and Seible 1994)

Line (2) represents a poorly confined column without lap splices in the plastic hinge region, for which the maximum strength is typically equal to the nominal strength. This model is suitable for the columns designed by pre-1971 design codes. Strength degradation will occur if the limit for line (1) or line (2) is reached due to crushing of core concrete and buckling of longitudinal reinforcement.

Line (3) represents degradation of a column with lap splices and poor confinement in the plastic hinge region, in which the nominal moment capacity will not be achieved. The strength starts degrading before $\mu_\Delta = 1$ to a residual flexural strength, M_r, which is a function of the magnitude of the axial load. The cause of the degradation is that the longitudinal bar in the lap splice region can not develop its yield force before slip and/or buckling occurs.

Line (4) represents degradation of a column with partially confined lap splices, in which the nominal moment capacity M_n can be reached and then a relatively small plastic plateau can be achieved before degradation begins. The degradation occurs when the extreme fiber compression strain ε_c is 0.002. This model indicates that the longitudinal bar in the lap splice region can develop its yield force before slip and/or buckling. The line degrades to M_r, parallel to line (3).

Both lines (3) and (4) show the typical flexural strength and ductility of column sections designed prior to 1971, in which the lap splices were in the range of 20 to 35 longitudinal bar diameters, and confinement reinforcement was inadequate, typically No. 4 (13 mm) reinforcement on 305 mm centers. In this report, a column behavior model, shown in Figure 5, is described. It should be noted that strain hardening in this model is neglected. The hysteretic rule is discussed subsequently.

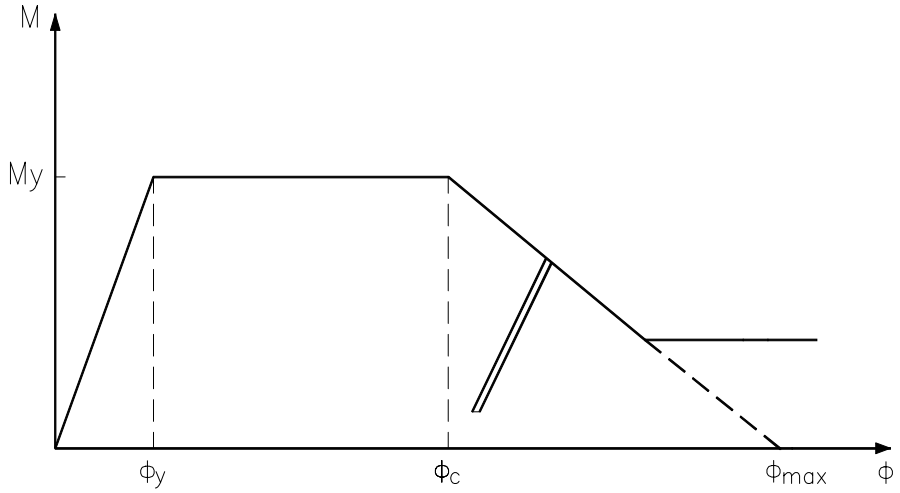

Figure 5. Moment vs. curvature relation of the element

3.1.1 Damage Coefficient

To derive the stiffness matrix for the softening stage, a damage coefficient, D, is introduced. The damage coefficient is defined such that a value of 0 indicates no damage while a value of 1 means total damage. Failure of actual components is observed to occur at an intermediate value of damage, $D_{\max}$. Therefore, during the evolution of softening, the damage coefficient is equal to

$$D = \frac{\theta_p - \theta_{cp}}{\theta_{\max} - \theta_{cp}}, \quad 0 \le D \le D_{\max} \le 1 \tag{1}$$

where θ_p is total plastic rotation angle, θ_{cp} is the critical plastic rotation angle that indicates the point at which softening begins, and $\theta_{\max}$ is the maximum theoretical plastic rotation angle. θ_{cp} and $\theta_{\max}$ may be calculated through the following formula:

$$\theta_{cp} = l_p \cdot (\phi_c - \phi_y) \tag{2}$$

$$\theta_{\max} = l_p \cdot (\phi_{\max} - \phi_y) \tag{3}$$

where l_p is plastic hinge length and $\phi_{\max}$ is the curvature for which the maximum moment capability is equal to zero, theoretically. Thus, according to the definition of the damage coefficient, at any point during the softening stage, the maximum moment capacity is

$$M = (1 - D) M_y \tag{4}$$

where M_y is the yielding moment.

3.1.2 Yield Function

The form of the generalized yield surface used in *NEABS* is shown in Figure 6. The formula is given as

$$\left(\frac{M_{yu}}{M_{yp}}\right)^2 + \left(\frac{M_{zu}}{M_{zp}}\right)^2 = 1 \tag{5}$$

where M_{yu} and M_{zu} are the bending moment values about the *y* and *z*-axes, respectively, on the interaction surface for a fixed value of axial force, P_u. M_{yp} and M_{zp} are the ultimate bending moment values about the *y* and *z*-axes, respectively, for the same fixed value of P_u when M_y and M_z are applied separately. To consider the influence of axial force P_u, the following cubic equations are used to compute M_{yp} and M_{zp}:

$$M_{yp} = M_{y0} \cdot \left[1 + a_1\left(\frac{P_u}{P_0}\right) + a_2\left(\frac{P_u}{P_0}\right)^2 + a_3\left(\frac{P_u}{P_0}\right)^3\right], -P_0 \langle P_u \langle P_t \tag{6}$$

$$M_{zp} = M_{z0} \cdot \left[1 + b_1\left(\frac{P_u}{P_0}\right) + b_2\left(\frac{P_u}{P_0}\right)^2 + b_3\left(\frac{P_u}{P_0}\right)^3\right], -P_0 \langle P_u \langle P_t \tag{7}$$

where P_t is the ultimate axial tensile force, P_0 is the ultimate axial compressive force, M_{y0} and M_{z0} are yielding moments about the *y* and *z*-axes, respectively, in pure bending, and a_1, a_2, a_3, b_1, b_2, and b_3 are constants.

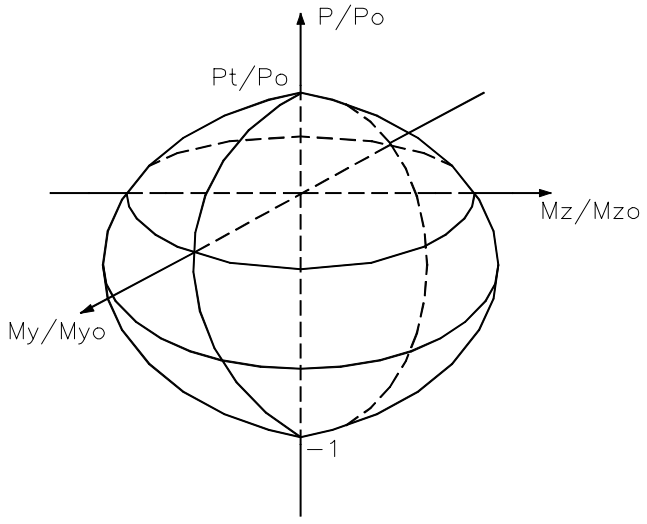

Figure 6. Generalized yield surface

One should note that the yield function mentioned above is only suitable for a perfectly plastic material, in that the yield stress level does not depend in any way on the degree of plastification. This means that the yield surface is fixed. For softening behavior, however, the yield surface is no longer unchanged in size, shape, or position with increasing plastification. The selected model for the evolution of softening in this paper is isotropic, in which the subsequent yield surface is a uniform contraction of the original one, as shown in Figure 7. The cause of the yield surface contraction is that the yield stress level at a point decreases with increasing plastic deformation.

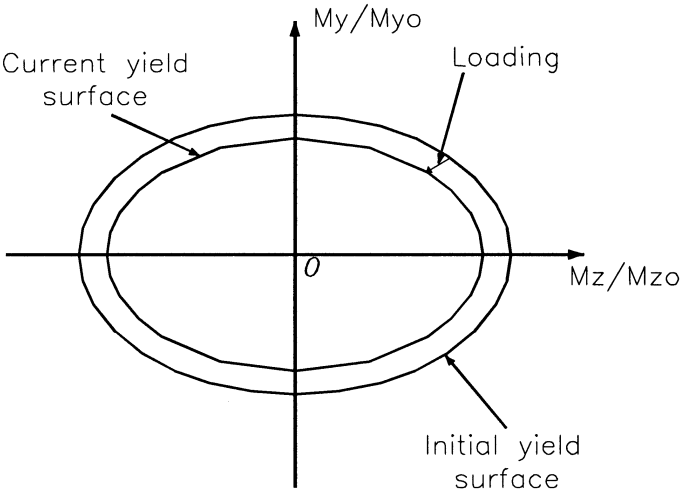

Figure 7. Yield curve of isotropic strain softening material for a fixed axial force

The yield function that also includes softening is defined as

$$\left(\frac{M_{yu}}{M_{yp}}\right)^2 + \left(\frac{M_{zu}}{M_{zp}}\right)^2 = (1-D)^2 \tag{8}$$

where D is the aforementioned damage coefficient and it is a function of plastic deformation. Because $(1-D)^2$ is less than or equal to one, the yield surface shrinks, providing a generalization of the curves of Priestley, Seible, and Chai (1992) for multiple dimensions.

3.1.3 Hysteresis Model

In this report, to imitate the actual behavior of reinforced concrete members subjected to cyclic deformation, a degradation of stiffness is considered. The application of stiffness degradation is illustrated by the moment vs. curvature curve in Figure 8. The loading, unloading, and reloading behavior are defined by the curve. The stiffness during unloading is assumed to be the same as the initial elastic stiffness, but the stiffness during reloading is allowed to degrade.

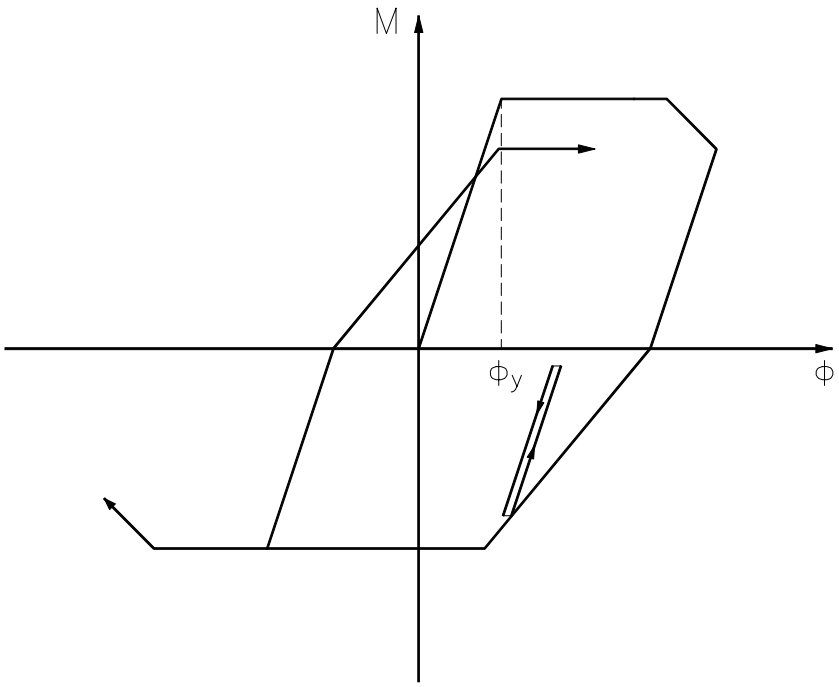

Figure 8. Hysteresis Model for the Beam-Column Element

The beam-column element is a three-dimensional element. During the elastic loading or unloading stage, as shown in Figure 8, the flexural capacities about the *y* and *z*-axes are modeled as being fully continuous with no stiffness degradation. However, during the elastic reloading stage, the end conditions about the *y* and *z*-axes are considered to be between fully continuous and fully hinged conditions, in which the degradation of stiffness is produced due to the damage. It should be noted that the approach is also based on the assumption that the shear and axial capacities remain intact. To obtain the degradation stiffness during the elastic reloading stage, the damage coefficient is used again to define the loss of elastic stiffness of the member due to damage. Detailed element derivations may be found elsewhere (Zhang 1996; Cofer et al. 1997).

3.2 Input Data for Plastic Hinge Model

To apply the Plastic Hinge Model, the yield function and the initiation and evolution of the damage parameter must be specified.

3.2.1 Yield Function

The expression for the yield function, which includes the interaction between bending moment and axial force, is given as Equations 6 and 7 for the two principal axes of the member. The required coefficients were determined by fitting a cubic curve to the axial force-bending moment strength interaction data computed for the specific column cross section upon attainment of a maximum concrete strain of $\varepsilon_{cu} = 0.002$. The computed interaction data was generated by a computer program which discretizes the column cross section and utilizes material constitutive laws developed by Burns and Seiss for steel and by Park and Kent for concrete, as reported by Park and Paulay (1975), in its force

equilibrium calculations. To facilitate this curve fitting, the following equations were developed, which force the curve to pass through the yield moment in pure bending (M_{y0} or M_{z0}) and the ultimate axial compressive capacity, P_0, and cause it to "peak" at M_m, as defined below.

$$
\begin{aligned}
a_0 &= 1 \\
a_1 &= \frac{1}{\alpha}\left[r^4 - qr(2-3r)\right] \\
a_2 &= \frac{1}{\alpha}\left[2r^3 - q(1-3r^2)\right] \\
a_3 &= \frac{1}{\alpha}\left[r^2 - q(1-2r)\right] \\
s &= \frac{1}{2a_3}\left[1 - a_1 - \sqrt{a_1^2 - 2a_1 - 4a_3 + 1}\right]
\end{aligned}
\tag{9}
$$

where:

$M_m \equiv$ maximum yield moment,

$P_m \equiv$ compressive axial force at maximum yield moment (positive); M_m and P_m would typically occur at the balance point of an axial force-bending moment curve for a square cross section,

$q \equiv \dfrac{M_m - M_{y0}}{M_{y0}}$,

$r \equiv \dfrac{P_m}{P_0}$, $r \neq 0.5$,

$\alpha \equiv r^2(1-r)^2$,

$s \equiv$ ratio $\dfrac{P_t}{P_0}$, required as input, where P_t is the ultimate axial tensile capacity.

Properties for bending about the z-axis are computed similarly. For the circular column considered here, the properties about the y-axis and the z-axis are identical. Figure 9 shows a comparison of the axial force-bending moment strength interaction data calculated for the column and the cubic curve obtained by the above procedure; the fit is quite close.

The region in the lap splice must be treated differently from the rest of the column because the longitudinal reinforcing steel may be unable to develop its full yield strength. The strength of a bar in a lap splice may be determined by postulating the full pattern of cracking that must develop to enable it to slide relative to the adjacent bar with which it is lapped. The tensile strength necessary to fracture this surface may be assumed to be equal to the direct concrete tension strength, i.e.,

$$f_t = 4\sqrt{f_c'} \text{ psi} \tag{10}$$

For a circular column, the total tensile force developed in a bar is:

$$T_b = f_t\left[\frac{\pi D'}{2n} + 2(d_b + c)\right]l_s \qquad (11)$$

where

n = number of longitudinal bars,
c = bar cover,
d_b = bar diameter,
D' = bar pitch circle diameter, and
l_s = splice length.

Then, a reduced effective yield stress of $f_s = \frac{T_b}{A_b}$ may be used in the moment-curvature analysis.

Using equations 10 and 11, f_t was computed to be 259.2 psi, T_b was computed to be 10.1 kips, resulting in an effective yield stress of 50.4 ksi. This value was used in the moment-curvature computer program to determine the section strength at the splice. In addition, a reduced amount of strain hardening was assumed. Pertinent data for the column and the splice are given in Table 1.

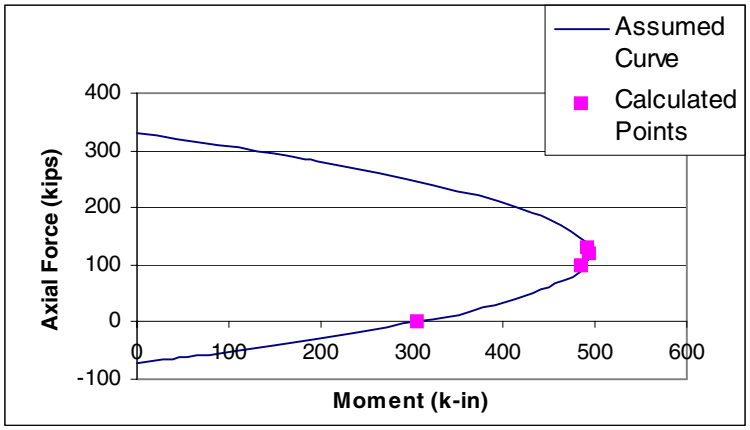

Figure 9. Calculated and assumed strength characteristics of the column

Table 1. Moment and axial force parameters for the column and the splice

	M_0 (K-in.)	P_0 (Kips)	M_m (K-in.)	P_m (Kips)	q	r	α
Column	306	330	494	119	0.614	0.360	0.0531
Splice	294	330	490	115	0.667	0.350	0.0518

Table 2. Coefficients for axial force-bending moment interaction

	a_0	a_1	a_2	a_3	s
Column	1	-3.51694	-5.31628	-0.79934	0.213335
Splice	1	-3.99298	-6.49039	-1.49741	0.189511

3.2.2 Hinge Properties

The curvature from nonlinear behavior in reinforced concrete members that is represented as a plastic hinge is typically assumed to occur within the equivalent plastic hinge length, l_p. Often, l_p is taken as half the depth of the member. However, in recent research by Chai et al. (1991), the following equation was suggested:

$$l_p = 0.08l + \chi d_b \tag{12}$$

where

$l =$ length from the critical section to the point of contraflexure,
$d_b =$ nominal diameter of the longitudinal reinforcement used in the member,
$\chi =$ 6 for grade 40 longitudinal reinforcement,
$=$ 9 for grade 60 longitudinal reinforcement.

For the column under investigation, the point of contraflexure was assumed to occur at the center of the member, resulting in l = 35 inches, d_b was 0.5 inches, and χ was set to a value of 6, resulting in a plastic hinge length, l_p = 5.8 inches.

Damage was only assumed to occur at the bottom of the column, which contained the lap splice. From the moment-curvature analysis, the yield moment, M_y, was 266 kip-inches while the residual moment, M_r, was determined to be 94 kip-inches. Their ratio is:

$$r_0 = \frac{M_r}{M_y} = 0.353 \tag{13}$$

Then,

$$D_{\max} = 1 - r_0 = 0.647 \tag{14}$$

Also, from the moment-curvature analysis, the curvature at yield, ϕ_y, the critical curvature at which damage initiates, ϕ_c, and the curvature for which moment is theoretically zero, ϕ_{max}, were specified. On the basis of equations 2 and 3, θ_{cp} and θ_{max} were computed as given in Table 3.

Table 3. Plastic hinge parameters

ϕ_y	ϕ_c	ϕ_{max}	θ_{cp}	θ_{max}
3.119×10^{-4}	8.502×10^{-4}	3.458×10^{-3}	3.122×10^{-3}	1.825×10^{-2}

.

3.2.3 Elastic Properties

For column behavior in the elastic range, the geometric moment of inertia for a circular section was used with an equivalent modulus of elasticity that was chosen on the basis of the moment-curvature analysis. For a required bending stiffness, *EI*, of 1.136×10^{6}, the equivalent modulus of elasticity was defined as 2314 ksi.

3.3 Analysis and Results

A model of the test specimen was developed, as shown in Figure 10. The support at the footing (node N1) was assumed to be fully fixed while the support at the base of the vertical strut (node N10) was assumed to be pinned. A hinge was assumed to exist at the connection between the vertical strut and the horizontal restraint beam (node N9). Relatively stiff elements were included to model the effect of the cap at the top of the column (elements M5 and M6) and the finite width of the horizontal restraint beam (element M8). Because of possible numerical difficulties arising from the fact that a degrading hinge at the base of the column results in a near mechanism, a weak horizontal spring element was added at the top right corner, node N8. Loading was applied as concentrated forces at node N6. The horizontal load was assumed to vary with time while the vertical load remained constant. Both monotonic and cyclic loading was applied. To remove inertial effects, mass was not included. However, a nominal amount of system damping was applied to improve numerical performance.

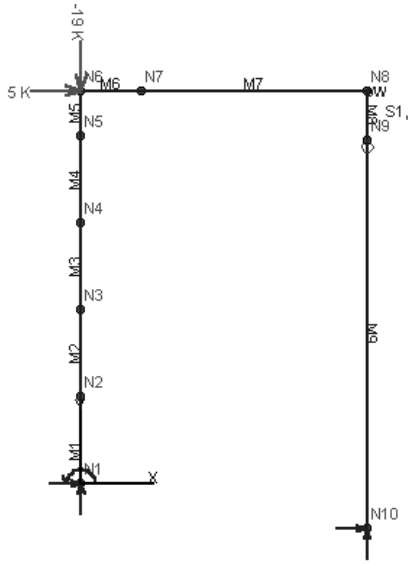

Figure 10. Model layout; horizontal load applied to show location and direction

For the monotonic loading case, the model was loaded horizontally in both the positive direction (push) and the negative direction (pull). The loading was ramped linearly from a zero value to a final value of 18 kips, which was chosen to be greater than the collapse load, as shown by experimental results. In the analyses, collapse is indicated by unbounded displacement or by divergence. Sample elastic deflected shapes are shown in Figure 11. The load-deflection curve is shown in Figure 12, while bending moment at the top and bottom of the column is shown in Figures 13 and 14, respectively.

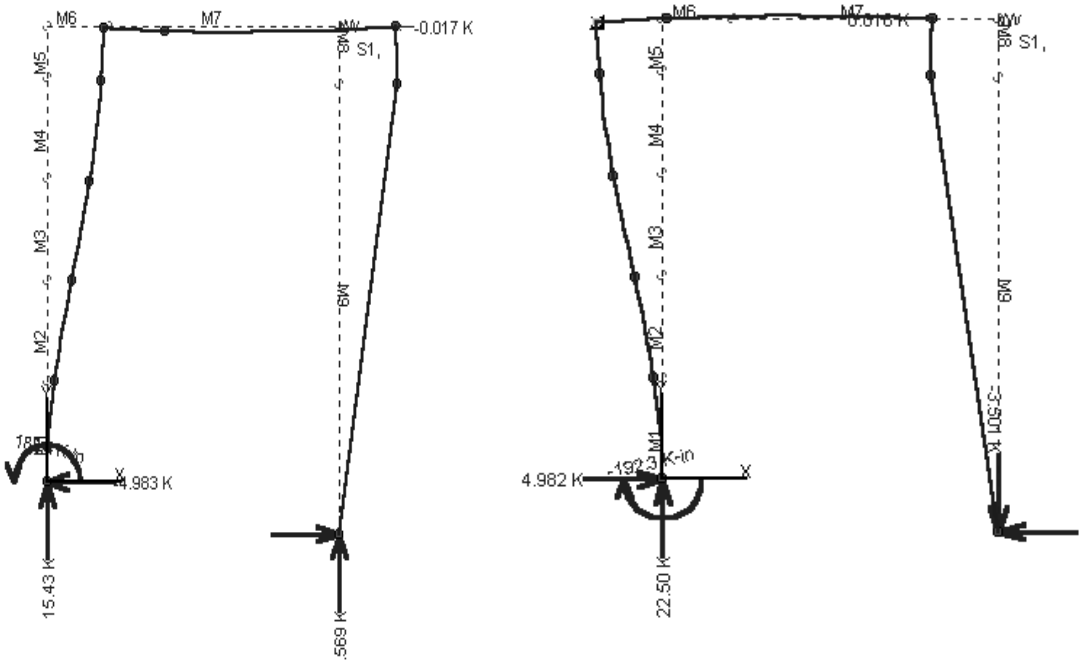

Figure 11. Example elastic deflected shapes for push and pull loading

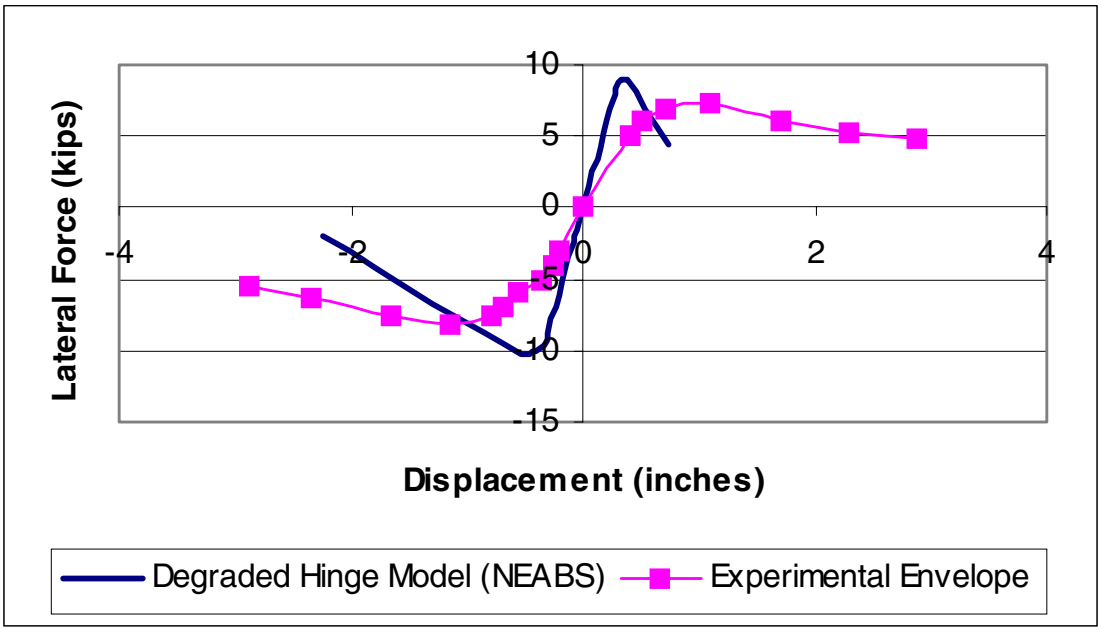

Figure 12. Lateral force vs. deflection for the test frame

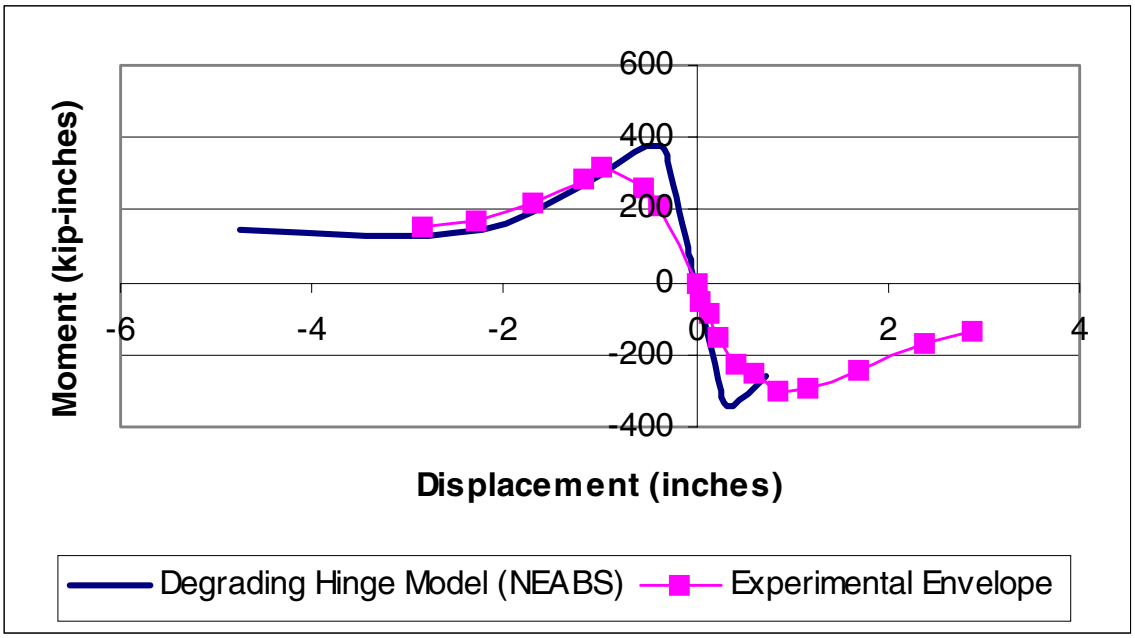

Figure 13. Bending moment at the base of the column

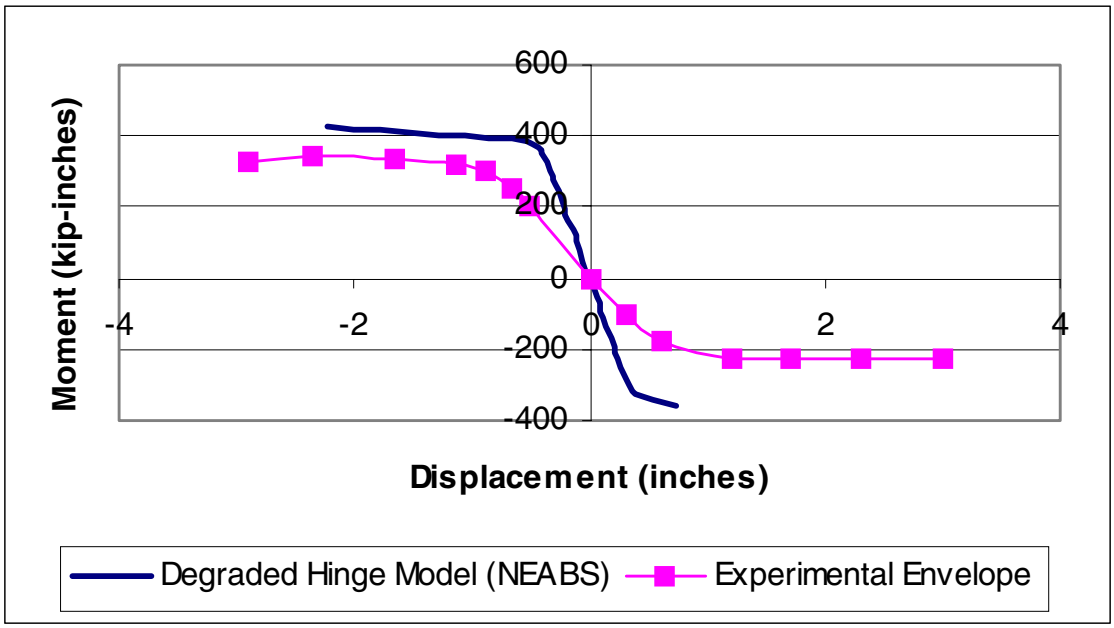

Figure 14. Bending moment at the top of the column

The effect of the splice at the base of the column is apparent when comparing the moment responses in Figures 13 and 14, in which the moment at the base degrades with damage. The difference between loading in the push and pull directions is shown to have a minor influence on strength due to an increase in column axial compression when pulled and a decrease in column axial compression when pushed. Numerical data for

peak loading is given in Table 4. Agreement for strength data is fairly close although the deflection data indicates that the model behavior is somewhat stiff. However, monotonic and cyclic results are not strictly comparable due to cyclic degradation, which is not considered in the analysis.

Table 4. Comparison of results from analysis and experiment

	Peak Applied Lateral Load (kips)	Lateral Deflection (inches)
Experimental (push)	8.0	0.8
Present Analysis (push)	8.9	0.39
Experimental (pull)	-7.7	-1.0
Present Analysis (pull)	-10.3	-0.53

For the cyclic loading case, an increasing series of ramped loads in alternating push and pull directions were applied, as given in Table 5. The load values were chosen to roughly correspond to the experimental procedure. The first cycle is slightly below the load for first yield while the second is somewhat higher than first yield and the third and fourth cycles are well above the strength of the system. Because there is no provision for cyclic degradation at plastic hinges in the model, only a single cycle of load was applied at each load level, as opposed to two cycles in the experimental tests. The time history data for lateral displacement, column shear, and top and bottom column moment are given in Figures 15 through 18, respectively. Hysteretic behavior is given in Figures 19, 20, and 21. Failure of the system was indicated by nonconvergence of the solution.

Table 5. Numerical value of load cycles

Cycle	Applied Lateral Load (kips)
1	± 7.42
2	±10.58
3	±15.88
4	±18.00

.

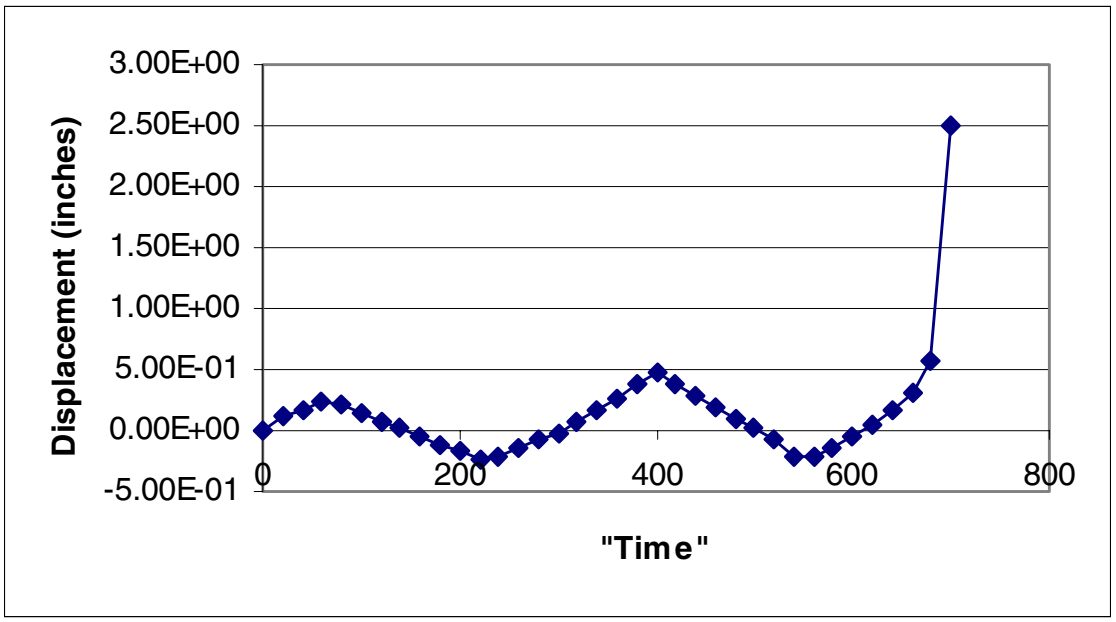

Figure 15. Time history of lateral deflection

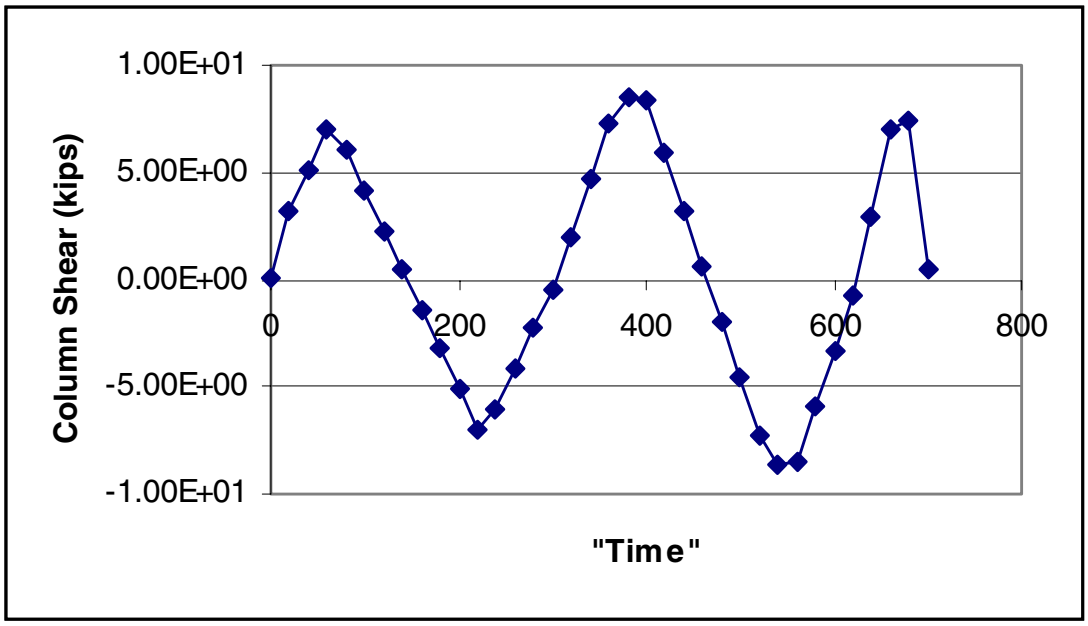

Figure 16. Time history of column shear

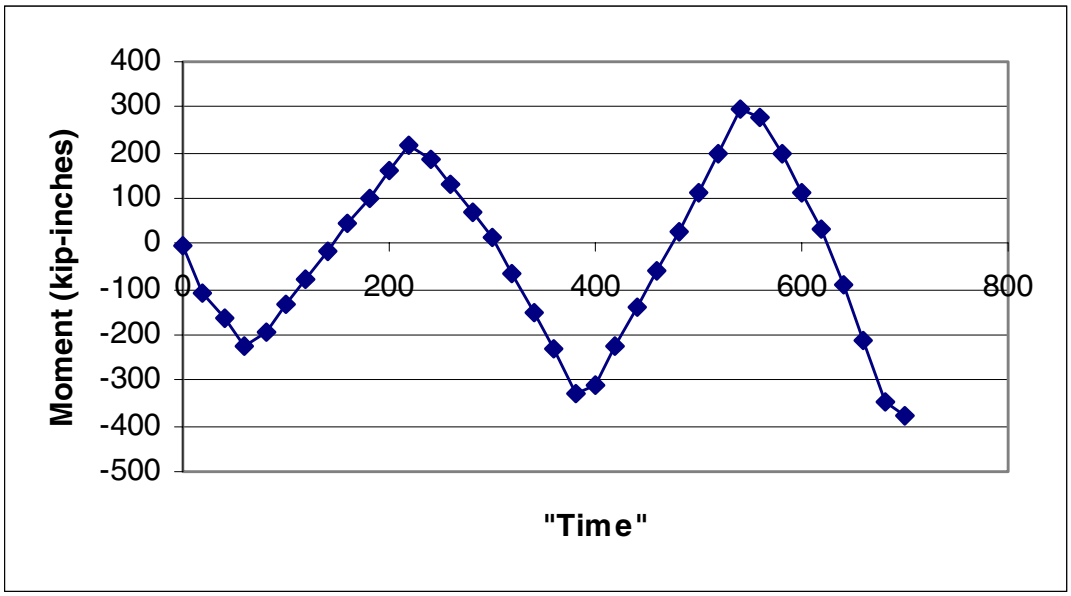

Figure 17. Time history of top column moment

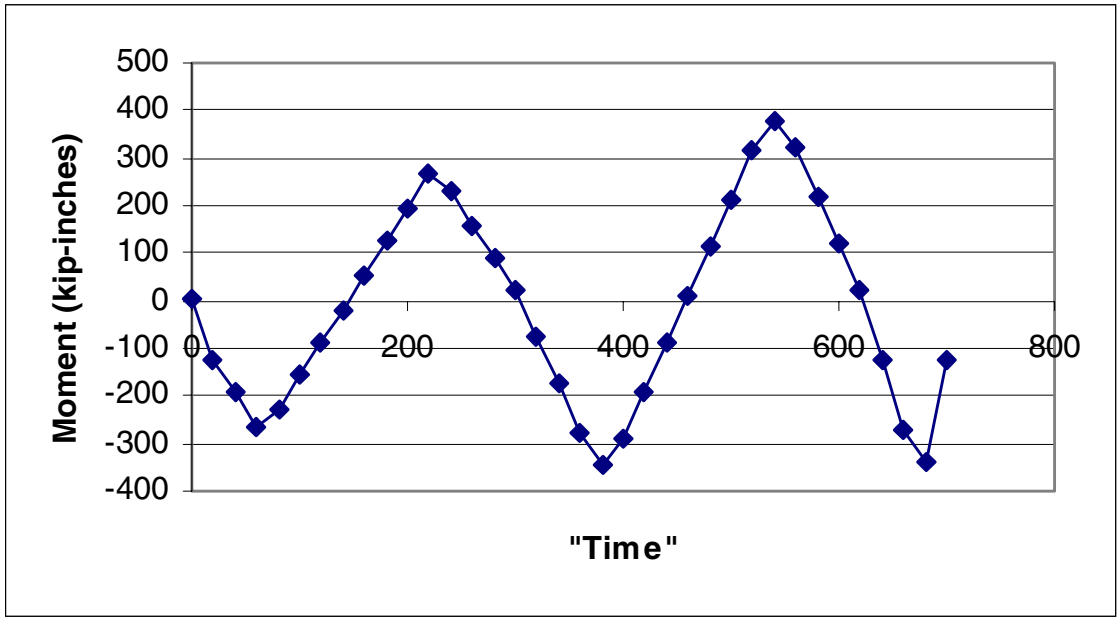

Figure 18. Time history of bottom column moment

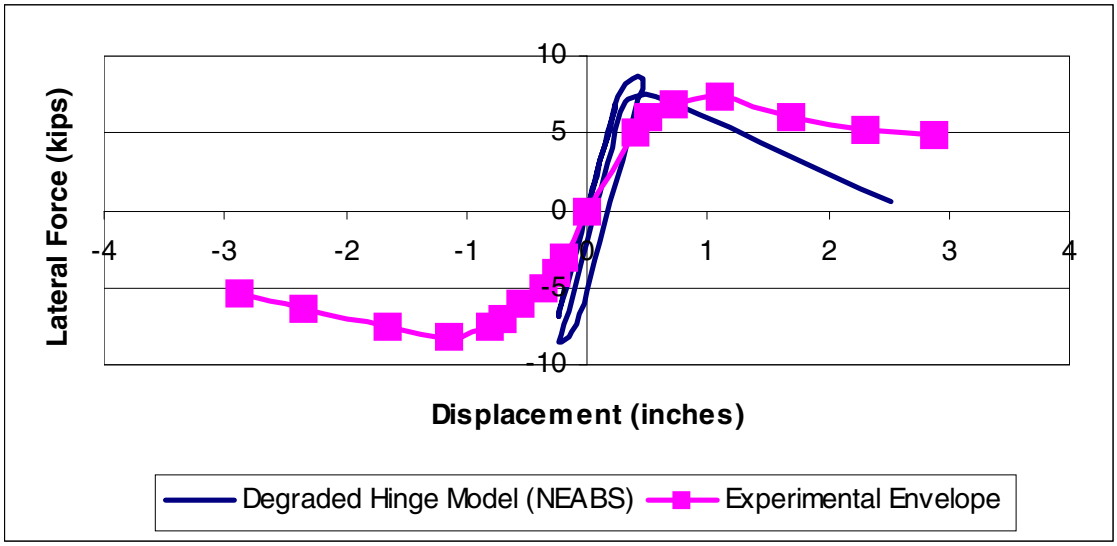

Figure 19. Hysteresis curve for the system

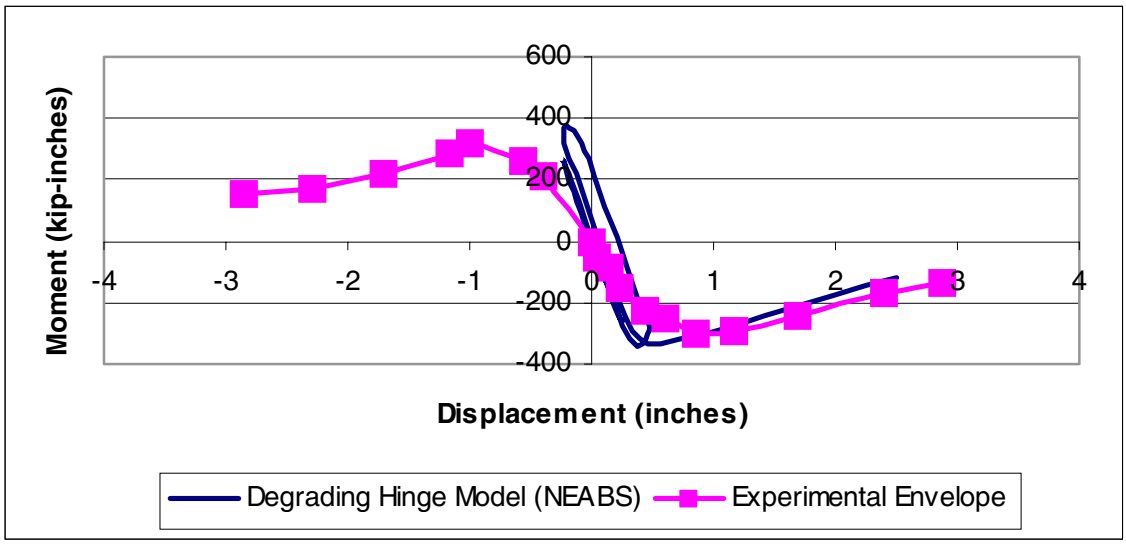

Figure 20. Hysteresis curve for bottom column moment

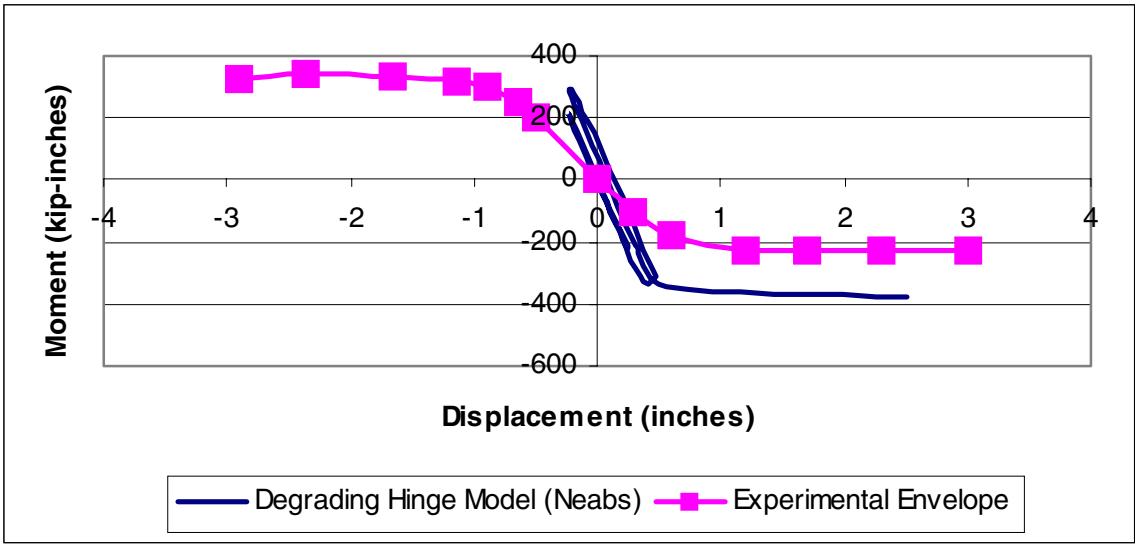

Figure 21. Hysteresis curve for top column moment

As expected, loading above the maximum capacity in the push direction resulted in a sharp drop in moment resistance at the base of the column which in turn resulted in near mechanism behavior. The results are quite similar to those obtained experimentally with recognition of the fact that displacement control was used for the tests while load control was used for the analyses. Lateral load capacity and column moment values are given in Table 6.

Table 6. Comparison of experimental and numerical results; plastic hinge model

	Experimental Value	Value from Present Analysis	Ratio of Results
Peak Lateral Force (push) (kips)	8.1	8.45	1.04
Peak Top Moment (kip-inches)	348	377	1.08
Peak Bottom Moment (kip-inches)	326	379	1.16

4 Software for the Fiber Beam Model

ABAQUS/standard is a commercially available, general-purpose finite element system with a wide variety of elements, materials, and procedures (*ABAQUS* 1998). For the analyses reported here, a nonlinear static procedure was employed using the Newton method for solution. Nonlinearities result from inelastic material behavior and from finite deformations. For the reinforced concrete column, a Timoshenko (i.e., shear-flexible) beam element was chosen with an assumed circular cross section and numerical integration through the beam depth.

Material properties were defined separately for the concrete and the steel reinforcing. The concrete material model is quite general, and it is intended for situations with low confining pressure and loadings that are relatively monotonic. The "smeared crack" assumption is employed, with the onset of cracking defined by the attainment of a "crack detection surface," which is a function of equivalent pressure stress and equivalent deviatoric stress. Gradual material softening is assumed, with the rate of softening determined by tension stiffening, allowing for the effects of interaction with reinforcement, or by crack opening displacement to consider consistent fracture energy release. The reduction in shear stiffness as a crack opens may also be specified.

For concrete loaded principally in compression, plasticity theory is used with a compression yield surface, similar to the crack detection surface, and assumed associated flow and isotropic hardening. These assumptions are considered to be inaccurate when concrete is subjected to significant pressure stress, but reasonable and computationally efficient otherwise. In addition, no attempt is made to include hysteretic behavior or a reduction in stiffness with cyclic loading. Concrete material properties are given in Tables 7, 8, and 9. Where specific values were not determined experimentally, accepted values from practice were used.

Table 7. Elastic-plastic material properties for concrete

Modulus of Elasticity (psi)	Poisson's Ratio	Uniaxial Compressive Yield Stress (psi)	Uniaxial Ultimate Compressive Stress (psi)	Plastic Strain at Ultimate Compressive Stress
3.72×10^6	0.18	1750	4200	0.0015

Table 8. Data to define the failure surface for concrete

Ratio of Ultimate Biaxial Compressive Stress to Ultimate Compressive Uniaxial Stress	Ratio of Uniaxial Tensile Failure Stress to Uniaxial Compressive Failure Stress	Ratio of Principal Plastic Strain at Ultimate Stress in Biaxial Compression to Plastic Strain at Ultimate Stress in Uniaxial Compression	Ratio of Tensile Principal Stress at Cracking to Tensile Cracking Stress under Uniaxial Tension
1.18	0.05	1.25	0.2

Table 9. Data to define retained tensile stress normal to a crack

Tensile Stress at Crack Initiation (psi)	Direct Cracking Strain at Complete Stress Release
210	0.0016

Reinforcing steel is included in the form of discrete bars at specific locations within the beam cross section. Only longitudinal reinforcing is considered. Elastic-plastic assumptions are employed with specific data used to specify hardening and/or softening in regions past initial yield. Continuous bars were assumed to be elastic-perfectly-plastic. To include the effect of the lap splice, the yield stress and post-yield behavior of bars in the splice region were adjusted, as previously described. Numerical values are given in Table 10. Note that softening is assumed to begin immediately upon yielding in the lap splice region.

Table 10. Reinforcing steel properties

	Continuous Reinforcing	Lap Splice
E (ksi)	29,000	29,000
σ_y (ksi)	52.0	50.4
Stress (ksi)/plastic strain	Assumed perfectly plastic	50.4/0.
		48.0/0.007
		10.0/0.015

4.1 Analysis and Results

Two models were developed and analyzed to determine the effect of mesh size. For the first model, denoted as *coarse*, eleven elements were used to represent the column. The length of the elements at the top and bottom were specified to match that of the plastic hinge, computed earlier to be 5.8 inches. The other model, denoted as *fine*, was composed of twenty-two elements, evenly spaced along the column. All other aspects of the model were equivalent to the degrading hinge model. Figures 22 and 23 show the layout of the models. Note that the Timoshenko beam elements have three nodes, resulting in a linear distribution of curvature.

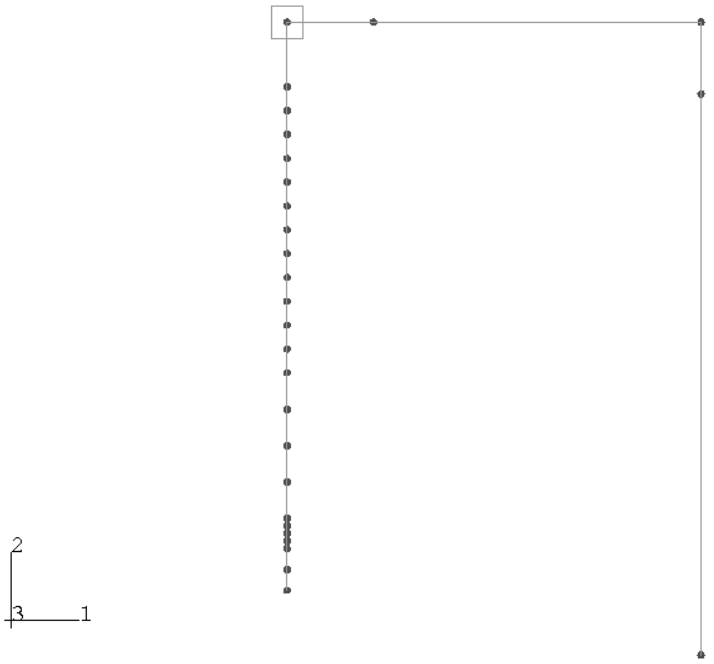

Figure 22. Mesh layout of the coarse model

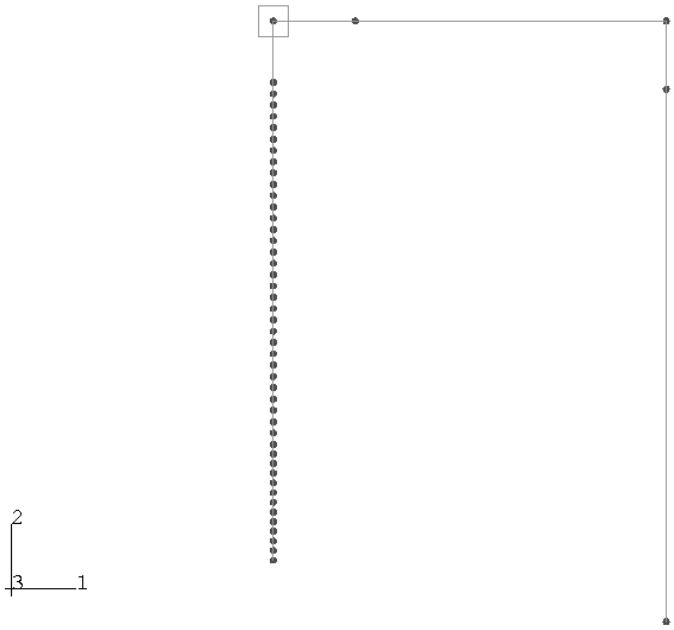

Figure 23. Mesh layout of the fine model

The axial compressive load was applied through a concentrated mass at the column top while lateral loading was applied via prescribed displacement. Because of the structure of the *ABAQUS* software, the mass was applied as an initial step and cyclic loading was applied with a number of independent steps in the push and then pull directions. For each step, the structure was loaded until a displacement of three inches was attained or a lack of convergence ended the solution. Curvature diagrams with exaggerated views of the deformed shape at the latter stages of deformation for the coarse and fine models are given in Figures 24 and 25. The figures show that, as damage progresses, curvature becomes concentrated at the hinge locations at the top and bottom of the column. The length of the hinge is always that of a single element.

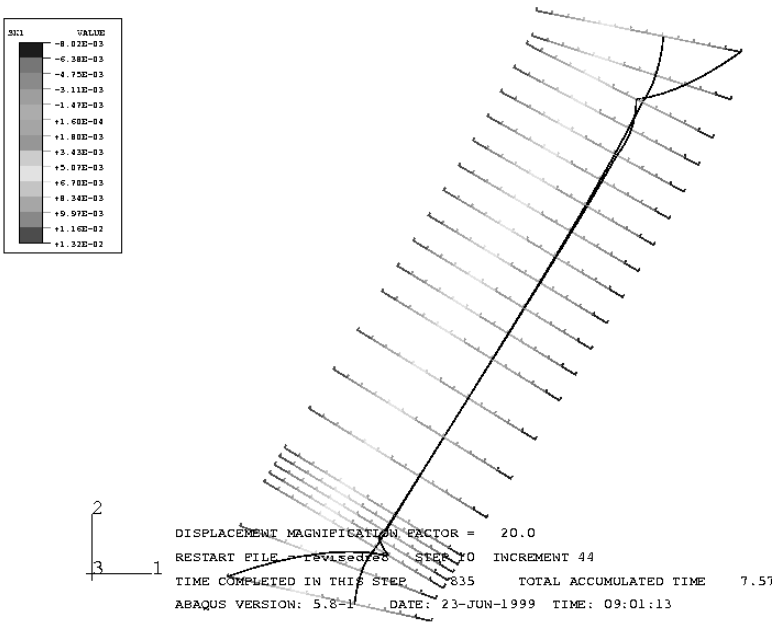

Figure 24. Curvature diagram and exaggerated deformed shape for the column; coarse mesh

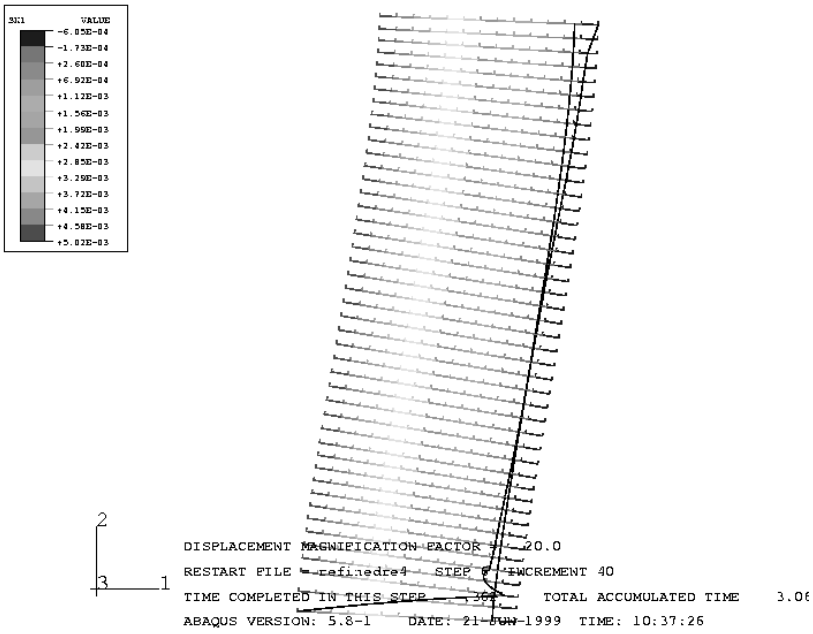

Figure 25. Curvature diagram and exaggerated deformed shape for the column; fine mesh

Comparisons of cyclic results for lateral load with those of the experiment are shown for both models in Figures 26 and 27. The response of the fine model is similar to that of the coarse model during the early stages of loading. However, with the formation of a plastic hinge at the bottom, the solution quickly diverged due to the reduced hinge length. For

the coarse model, values for the moment at the bottom and top of the column are shown in Figures 28 and 29. A comparison of peak numerical values is given in Table 11.

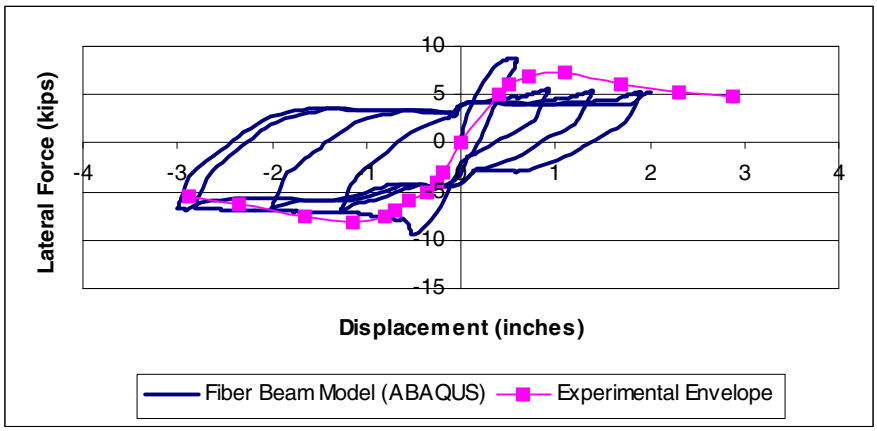

Figure 26. Hysteresis curve for the system; coarse model

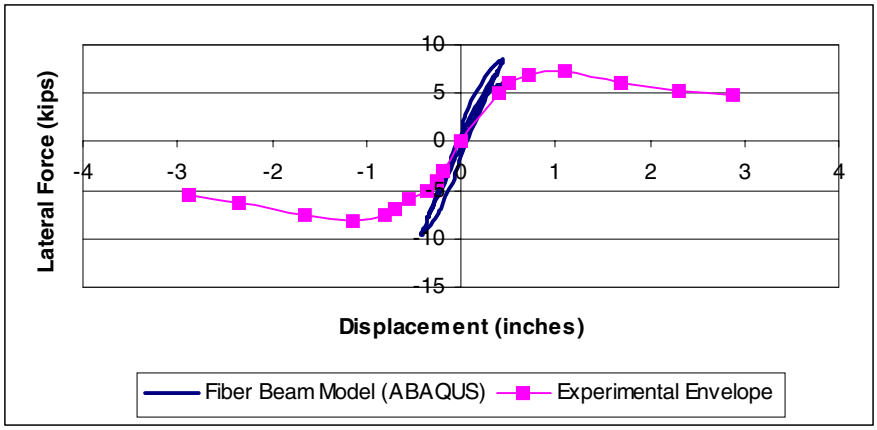

Figure 27. Hysteresis curve for the system; fine model

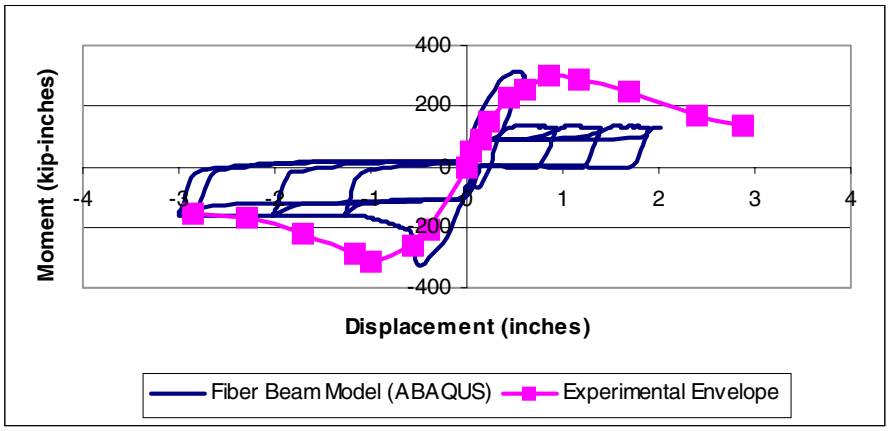

Figure 28. Hysteresis curve for bottom column moment; coarse model

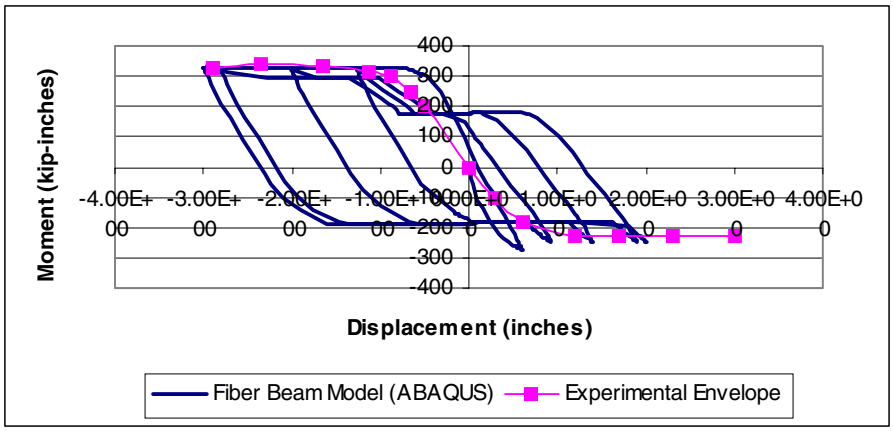

Figure 29. Hysteresis curve for top column moment; coarse model

Table 11. Comparison of peak numerical values for the coarse fiber beam model

	Experimental Value	Value from Present Analysis	Ratio of Results
Peak Lateral Force (push) (kips)	8.1	8.83	1.09
Peak Top Moment (kip-inches)	348	330	0.95
Peak Bottom Moment (kip-inches)	326	324	0.99

5 Software for Nonlinear Three-Dimensional Finite Element Analysis

ABAQUS/standard was also used for the detailed three-dimensional, finite element analysis of the column. The analysis procedure was essentially the same as that used for the fiber beam model, except that 20-node quadratic brick elements were used for the concrete, with embedded reinforcing steel. Material models and constants were also unchanged. The finite element model is shown in Figure 30. Note that a plane of symmetry was included. Also, proper constraints were applied at the interface between the solid elements at the top of the column and the beam element representing the rigid cap to result in a transfer of bending behavior.

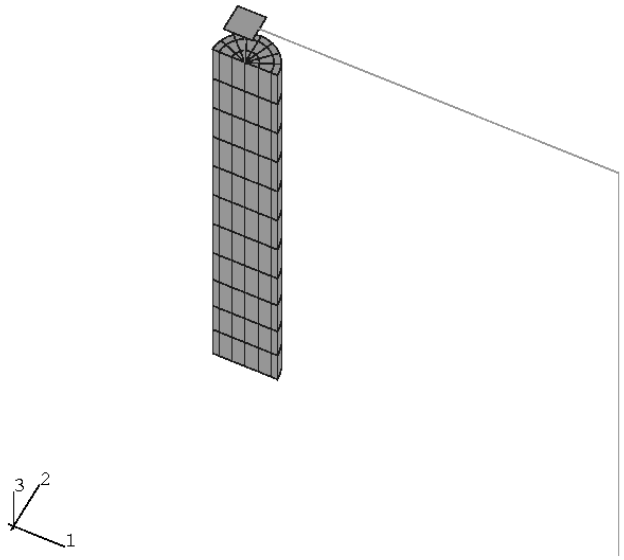

Figure 30. Finite element mesh for the three-dimensional finite element model

5.1 Analysis and Results

As with the fiber beam model, a concentrated mass was applied at the top of the column and lateral loading was applied through prescribed displacement until lack of convergence ended the solution. The displaced shape for a typical case is shown in Figure 31. Contours of vertical stress, vertical strain, and crack opening strain are shown in Figures 32-34. Stress is given in units of psi. The initiation of cracking is assumed to occur at a tensile stress level of 210 psi, while complete stress release occurs at a strain level of 0.0016. From the figures, it is apparent that, although compressive failure has not yet occurred, cracking is widespread throughout the tensile portion of the column, with a localized concentration at the top. The concentrated cracking at the top is

responsible for the nonconvergence that inhibited the ability of the model to continue significantly into the plastic range, as shown in Figure 35.

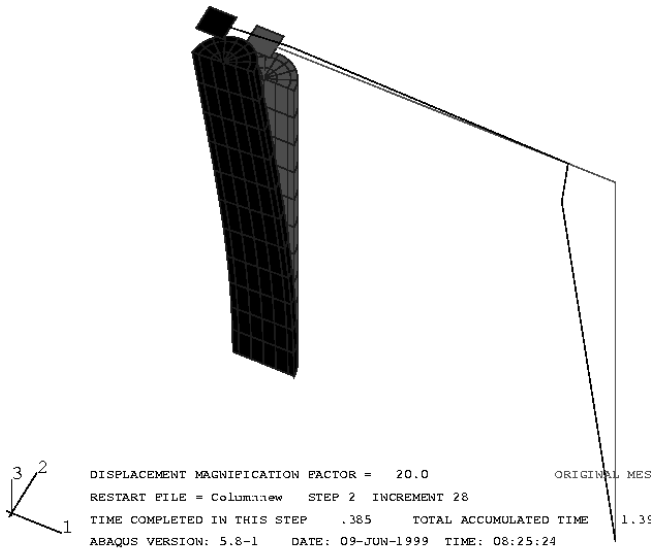

Figure 31. Deformed shape, three-dimensional finite element model

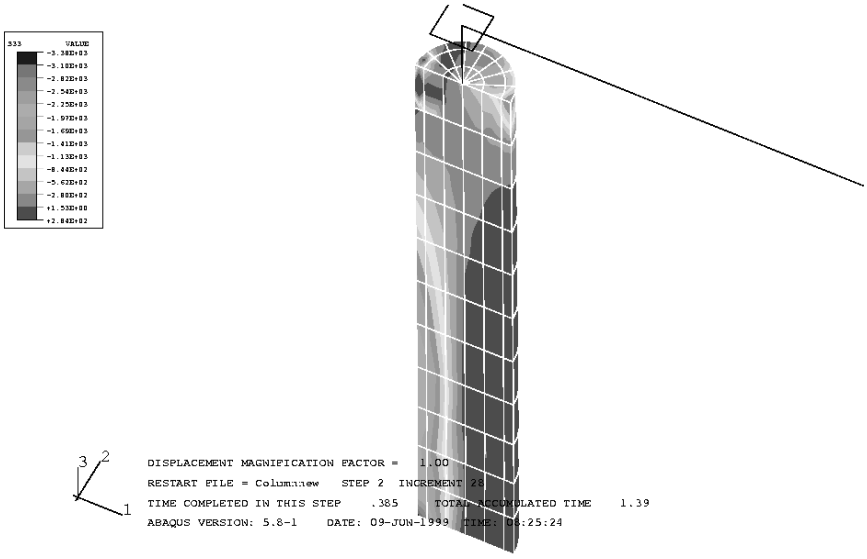

Figure 32. Contours of vertical stress

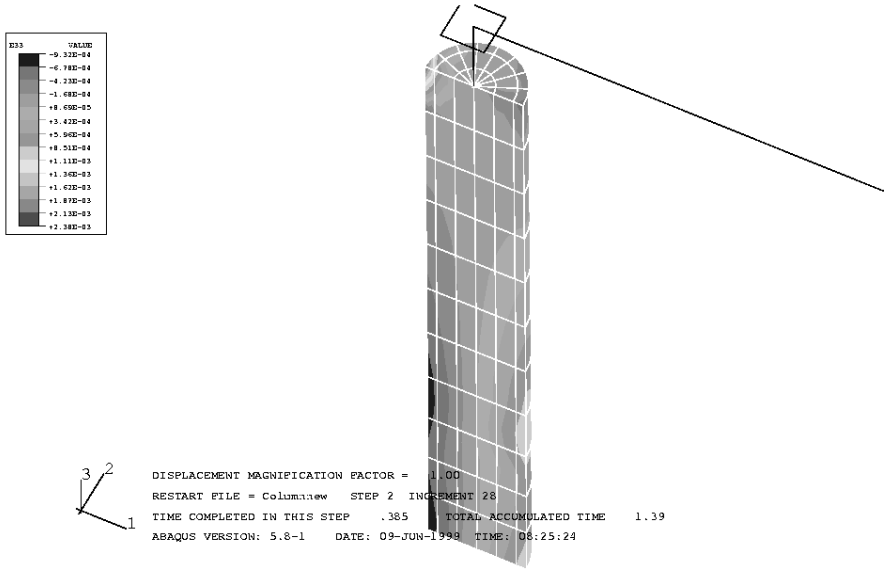

Figure 33. Contours of vertical strain

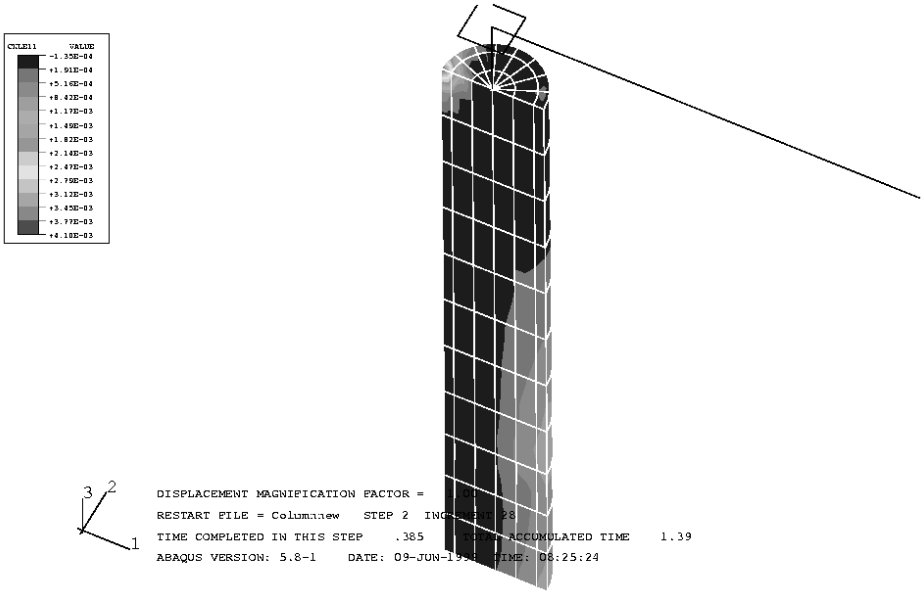

Figure 34. Contours of crack-opening strain

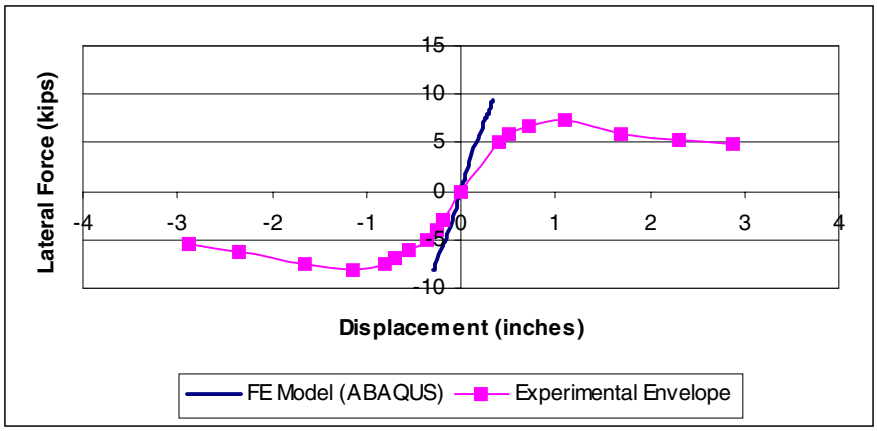

Figure 35. System behavior, three-dimensional finite element model

As with previous models, Figure 35 shows that the column has an initial stiffness that is somewhat higher than that observed experimentally. With the fiber beam model, however, the stiffness for subsequent cycles compared quite well, suggesting that the stiffness of the actual column is significantly affected by initial cracking. For monotonic loading, the stiffness of all three models compared closely, as shown in Figure 36.

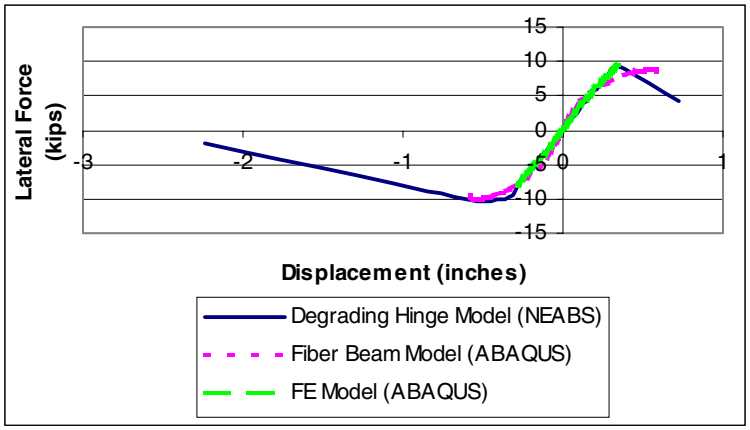

Figure 36. A comparison of system stiffness for all models

6 Discussion and Conclusions

For the work of this report, a benchmark reinforced concrete column test for cyclic behavior was analyzed using existing software and techniques to determine their ability to obtain reasonable numerical simulations. A model based on classical frame elements with degrading hinges, one based on Timoshenko beam elements and fiber concepts for applying material behavior, and a detailed three-dimensional finite element model were considered. For each analysis, common engineering practice was used to obtain the required input data, based solely on cylinder strength information for concrete and coupon tests for steel. In general, the results were quite accurate for all methods, with varying degrees of robustness, as described below.

6.1 Degrading Hinge Model

This was the simplest model, but it required the most effort to obtain input data, using separate software and engineering assumptions to define moment-curvature and hysteretic behavior for the plastic hinges. However, the solution was accurate and quite robust as long as the hinge has the ability to degrade.

6.2 Fiber Beam Model

The input for this model was more basic than that of the degrading hinge model in that it consisted mainly of material information. Although the material model is rather complex, the use of default values for most input items led to reasonable results. A quadratic Timoshenko beam element was chosen, which resulted in a linear variation of curvature along the length of the element and included shear deformation, both of which seemed significant. As with many applications in finite element analysis dealing with failure, the results were mesh dependent. However, with an appropriate estimate of the plastic hinge length in the column, results were obtained that were quite accurate.

The initial stiffness of the column model was significantly higher than that observed experimentally, but after the occurrence of cracking during the first cycle, they were quite close. Thus, a reduction of initial section properties to consider residual cracking is probably in order, particularly for elastic analysis. Often, analysts choose to use half of the gross moment of inertia for the section.

The force, displacement, and moment results from this model were quite close to those obtained experimentally. In addition, the solution was efficient and relatively robust.

6.3 Three-Dimensional Finite Element Model

Although the effort for model development and the computer requirements for this model were much greater than for the others, detailed output information regarding stress and

strain distribution, along with cracking, is available. However, the solution did not converge beyond initial cracking, rendering it useless for evaluating hysteretic behavior that involves gross yielding of reinforcement or crushing of concrete.

6.4 Conclusions

Only a single structure was analyzed for the work of this report using three specific programs, and any conclusions that are drawn are not necessarily universal. However, the following may be surmised:

1. The degrading hinge model is the simplest and most robust of the three considered, making it the most practical for the analysis of large structures. Although it was not the best performer, the results from the model were reasonably accurate as long as the hinge model includes the effect of axial force in the column and degradation, and as long as care is taken in defining yield properties, hysteretic behavior, and hinge length.

2. The fiber beam model was the best overall performer with regard to accuracy, but it was not as robust as the degrading hinge model. In addition, the solution was sensitive to the degree of mesh refinement.

3. The three-dimensional finite element model was unable to provide usable results due to numerical difficulties. Other material models and crack algorithms may offer improved performance, but the computational power and modeling effort required make this approach impractical for anything beyond detailed component analysis.

In conclusion, reasonable engineering solutions for the cyclic behavior of reinforced concrete structures appear attainable with existing techniques as long as the analyst understands the assumptions and limitations inherent in them and takes proper care in developing the input data and interpreting the results.

References

ABAQUS/standard user's manual. Version 5.8. 1998. Pawtucket, RI: Hibbitt, Karlsson, and Sorensen, Inc.

Chai, Y. H., M. J. N. Priestley, and F. Seible 1991. Flexural retrofit of circular reinforced concrete bridge columns by steel jacketing. Report no. SSRP 91/06. October. San Diego, Calif.: Structural Systems Research Project, University of California.

Cofer, W. F., Y. Zhang, and D. I. McLean. 1997. Analytical evaluation of retrofit strategies for multi-column bridges. Final technical report no. WA-RD 427.1, June. [Olympia]:Washington State Department of Transportation.

Imbsen, R., R. V. Nutt, and J. Penzien. 1978. Seismic response of bridges — Case Studies. Report no. FHWA-RD-78-157. Berkeley, Calif.: Earthquake Engineering Research Center, University of California.

Imbsen, R., and J. Penzien. 1986. Evaluation of energy absorption characteristics of highway bridges under seismic conditions. Volume I, UCB/EERC-84/17, September. Berkeley, Calif.: Earthquake Engineering Research Center, University of California..

Jaradat, O. A., D. I. McLean, and M. L. Marsh. 1998. Performance of existing bridge columns under cyclic loading — Part I: Experimental results and observed behavior. *ACI Structural Journal*. 95(6): 695–704.

Kawashima, K. and J. Penzien 1976. Correlative investigations on theoretical and experimental dynamic behavior of a model bridge structure. Report no. FHWA-RD-77-57. Berkeley, Calif.: Earthquake Engineering Research Center, University of California.

McGuire, J. W., W. F. Cofer, D. I. McLean, and M L. Marsh 1994. Analytical modeling of spread footing foundations for seismic analysis of bridges. *Transportation Research Record 1447*: 80–92. TRB.

Park, R. and T. Paulay (1975). *Reinforced Concrete Structures*, John Wiley and Sons, New York.

Priestley, M.J.N., F. Seible, and Y. H. Chai (1992). "Design Guidelines for Assessment Retrofit and Repair of Bridges for Seismic Performance," Report No. SSRP-92/01, Department of Applied Mechanics and Engineering Sciences, University of California, San Diego, California 266.

Priestley, M. J. N., and F. Seible (1994). "Seismic Assessment of Existing Bridges," Seismic Design and Retrofitting of Reinforced Concrete Bridges, *Proceedings* of the Second International Workshop, Queenstown, New Zealand, August, 1994, pp. 447-471.

Tseng, W. and J. Penzien (1973). "Analytical Investigations of the Seismic Response of Long Multiple-Span Highway Bridges," Earthquake Engineering Research Center, University of California, Berkeley, CA.

Zhang, Y. (1996). "Analytical Evaluation of Retrofit Strategies for Multi-Column Bridges," Ph.D. Dissertation, Department of Civil and Environmental Engineering, Washington State University, Pullman, WA, USA.

Zhang, Y., Cofer, W. F., and McLean, D. I. (1999). "Analytical Evaluation of Retrofit Strategies for Multi-Column Bridges," *Journal of Bridge Engineering*, Vol. 4, No. 2, pp. 143-150.

PEER REPORTS

PEER reports are available from the National Information Service for Earthquake Engineering (NISEE) and from the National Technical Information Service (NTIS). To order PEER reports, please contact the Pacific Earthquake Engineering Research Center, 1301 South 46th Street, Richmond, California 94804-4698. Tel.: (510) 231-9468; Fax: (510) 231-9461.

PEER 1999/07 *Documentation of Strengths and Weaknesses of Current Computer Analysis Methods for Seismic Performance of Reinforced Concrete Members***.** William F. Cofer. November 1999. $15.00

PEER 1999/06 *Rocking Response and Overturning of Anchored Equipment under Seismic Excitations.* Nicos Makris and Jian Zhang. November 1999. $15.00

PEER 1999/05 *Seismic Evaluation of 550 kV Porcelain Transformer Bushings.* Amir S. Gilani, Andrew S. Whittaker, Gregory L. Fenves, Eric Fujisaki. October 1999. $15.00

PEER 1999/04 *Adoption and Enforcement of Earthquake Risk-Reduction Measures.* Peter J. May, Raymond J. Burby, T. Jens Feeley, and Robert Wood. $15.00

PEER 1999/03 *Task 3 Characterization of Site Response General Site Categories*. Adrian Rodriguez-Marek, Jonathan D. Bray, and Norman Abrahamson. February 1999. $20.00

PEER 1999/02 *Capacity-Demand-Diagram Methods for Estimating Seismic Deformation of Inelastic Structures: SDF Systems*. Anil K. Chopra and Rakesh Goel. April 1999. $15.00

PEER 1999/01 *Interaction in Interconnected Electrical Substation Equipment Subjected to Earthquake Ground Motions.* Armen Der Kiureghian, Jerome L. Sackman, and Kee-Jeung Hong. February 1999. $20.00

PEER 1998/08 *Behavior and Failure Analysis of a Multiple-Frame Highway Bridge in the 1994 Northridge Earthquake.* Gregory L. Fenves and Michael Ellery. December 1998. $20.00

PEER 1998/07 *Empirical Evaluation of Inertial Soil-Structure Interaction Effects.* Jonathan P. Stewart, Raymond B. Seed, and Gregory L. Fenves. November 1998. $26.00

PEER 1998/06 *Effect of Damping Mechanisms on the Response of Seismic Isolated Structures*. Nicos Makris and Shih-Po Chang. November 1998. $15.00

PEER 1998/05 *Rocking Response and Overturning of Equipment under Horizontal Pulse-Type Motions.* Nicos Makris and Yiannis Roussos, October 1998. $15.00

PEER 1998/04 *Pacific Earthquake Engineering Research Invitational Workshop Proceedings, May 14–15, 1998: Defining the Links Between Planning, Policy Analysis, Economics and Earthquake Engineering.* Mary Comerio and Peter Gordon. September 1998. $15.00

PEER 1998/03 *Repair/Upgrade Procedures for Welded Beam to Column Connections.* James C. Anderson and Xiaojing Duan, May 1998. $33.00

PEER 1998/02 *Seismic Evaluation of 196 kV Porcelain Transformer Bushings.* Amir S. Gilani, Juan W. Chavez, Gregory L. Fenves, and Andrew S. Whittaker, May 1998. $20.00

PEER 1998/01 Unassigned.